Environment International 135 (2020) 105376

Contents lists available at ScienceDirect

Environment International

journal homepage: www.elsevier.com/locate/envint

(Im)mobilization and speciation of lead under dynamic redox conditions in a contaminated soil amended with pine sawdust biochar

Jingzi Beiyuan[a,b,c], Yasser M. Awad[c,d], Felix Beckers[c], Jianxu Wang[e,c], Daniel C.W. Tsang[b,**], Yong Sik Ok[f,***], Shan-Li Wang[g], Hailong Wang[a,h], Jörg Rinklebe[c,i,*]

[a] Biochar Engineering Technology Research Center of Guangdong Province, School of Environmental and Chemical Engineering, Foshan University, Foshan 528000, China
[b] Department of Civil and Environmental Engineering, The Hong Kong Polytechnic University, Hung Hom, Kowloon, Hong Kong, China
[c] University of Wuppertal, School of Architecture and Civil Engineering, Institute of Foundation Engineering, Water- and Waste-Management, Soil- and Groundwater-Management, Pauluskirchstraße 7, 42285 Wuppertal, Germany
[d] Faculty of Agriculture, Suez Canal University, Ismailia 41522, Egypt
[e] State Key Laboratory of Environmental Geochemistry, Institute of Geochemistry, Chinese Academy of Sciences, 550082 Guiyang, China
[f] Korea Biochar Research Center & Division of Environmental Science and Ecological Engineering, Korea University, Seoul 02841, Republic of Korea
[g] Department of Agricultural Chemistry, National Taiwan University, Taipei 106, Taiwan, ROC
[h] Key Laboratory of Soil Contamination Bioremediation of Zhejiang Province, Zhejiang A&F University, Hangzhou, Zhejiang 311300, China
[i] Department of Environment, Energy and Geoinformatics at Sejong University, 98 Gunja-Dong, Guangjin-Gu, Seoul, Republic of Korea

ARTICLE INFO

Handling Editor: Da Chen

Keywords:
Immobilization/stabilization
Lead dissolution/mobility
Paddy soil
XANES spectroscopy
Black carbon

ABSTRACT

Biochar can reduce the mobility and availability of potentially toxic elements (PTEs) in soils and improve soil properties. However, immobilization efficiencies of biochar can be varied according to environmental conditions, such as pH and redox potential (E_h), especially for soils under flood-dry cycles. In the current study, biochar produced at 300 and 550 °C (referred as BC300 and BC550, respectively) and its feedstock (pine sawdust biomass, BM) were used to amend a lead (Pb)-contaminated soil under pre-defined redox windows (from −300 to +250 mV). Key features of the soil-solution were evaluated in detail, including pH, dissolved organic carbon, sulphate, and dissolved Al, Fe, and Mn. The BC550 reduced the amount of dissolved Pb and showed a different pattern of E_h-pH in the soil slurry compared with BM and BC300. This might be attributed to its higher alkalinity and surface area. The highest amount of dissolved Pb was found at slightly anoxic conditions (−100 to 0 mV) in CS (control soil), S&BM (soil amended with BM), and S&BC300 (soil amended with BC300), which could be associated with the dissolution of Fe/Mn oxides. Moreover, the fitting results of Pb X-ray absorption fine structure (XAFS) indicated that the proportion of $Pb(CH_3COO)_2$ was decreasing when changing from anoxic to oxic condition in S&BC300, while the Pb speciation pattern in soil was stable in S&BC550. These results suggested that BC550 is more suitable amendment for Pb immobilization than BM and BC300 in this study. In addition, biochar produced at higher temperatures can be more stable so it can be suitable for remediation of Pb-contaminated soils which are frequently flooded.

1. Introduction

Organic amendments produced from waste materials (e.g. biochar and biomass) have captured great interest in different areas, for example, being as catalysts in biorefinery, adsorbents for removing contaminants in water, and immobilizers for potentially toxic elements (PTEs) in contaminated soils (Ahmad et al., 2016a; Beiyuan et al., 2017b; Sun et al., 2019; Yu et al., 2019). Large numbers of studies found that biochar can decrease the mobility, leachability, and availability of the PTEs in contaminated soils (Beckers et al., 2019; Beiyuan et al., 2018; Igalavithana et al., 2019), immobilize PTEs in residual soil after washing (Shen et al., 2019b; Yoo et al., 2018), improve soil fertility (El-Naggar et al., 2019a), reduce plant uptakes of PTEs (Xing et al., 2020), and promote plant growth and yield (Rizwan et al., 2016). The feedstock and pyrolysis temperature of biochar are the two significant factors controlling its immobilization effects on PTEs (Jin et al.,

* Corresponding author.
** Corresponding author.
*** Corresponding author.
E-mail addresses: dan.tsang@polyu.edu.hk (D.C.W. Tsang), yongsikok@korea.ac.kr (Y.S. Ok), rinklebe@uni-wuppertal.de (J. Rinklebe).

https://doi.org/10.1016/j.envint.2019.105376
Received 18 September 2019; Received in revised form 18 November 2019; Accepted 29 November 2019

2016; Li et al., 2016b). These two factors primarily determine the key physiochemical characteristics of biochar, such as pH, cation exchange capacity (CEC), surface area, micro-porous structure, organic carbon content, surface functional groups, and inorganic minerals (Lu et al., 2017; Mohan et al., 2014; Xiong et al., 2017). Notably, using the same feedstock, biochar production with high pyrolysis temperatures (i.e. > 500 °C) can decompose most of the organic components, leading to biochar with a higher alkalinity and less oxygen-containing functional groups (Rajapaksha et al., 2014).

Under varied environmental factors (e.g. pH, redox conditions (E_h), temperature, and microbial activities), distribution and speciation of the PTEs can be strongly influenced and subsequently affected their mobility and availability (Beiyuan et al., 2016; El-Naggar et al., 2019b; Shaheen et al., 2016). Among the factors, E_h is particularly significant for determining the mobility and availability of PTEs, because it directly or indirectly influence pH, dissolved organic carbon (DOC), redox chemistry of iron (Fe), manganese (Mn), sulfur (S), and nitrogen (N), and microbial activities in a flooded soil system (Frohne et al., 2015; Schulz-Zunkel et al., 2015). Most importantly, under anaerobic conditions (i.e. low E_h), PTEs associated with Fe/Mn oxides (the relevant standard redox couples are Fe(II)/Fe(III) and Mn(II)/Mn(IV)) release because of the reduction-induced dissolution of the oxides (Antoniadis et al., 2017; Du Laing et al., 2009a; Du Laing et al., 2009b). Besides, under anaerobic conditions, the PTEs can be immobilized by forming insoluble precipitates with sulfide which generated by reduction of sulfate (SO_4^{2+}/S^{2-}) (Du Laing et al., 2009b).

Lead (Pb) is extremely toxic and it is classified as Class B2 (a probable human carcinogen) according to the Integrated Risk Information System of US EPA. Under dynamic E_h, the mobility of Pb in soils is affected by the interaction with (1) Fe/Mn oxides by sorption and/or co-precipitation (especially for Mn oxides); (2) carbonates and phosphates; (3) clay minerals and soil organic matter (SOM) via sorption or complexation (Rinklebe et al., 2016b; Yang et al., 2018). Different types of biochar showed great capacity on Pb immobilization via electrostatic interaction, cation exchange, complexation, and precipitation (Ahmad et al., 2016b; Igalavithana et al., 2019). The addition of biochar can alter the speciation of Pb in soils and therefore change Pb immobilization effects. For example, Moon et al. (2013) reported that with the addition of soybean stover-derived biochar, the amount of Pb in stable chloropyromorphite ($Pb_5(PO_4)_3Cl$) form and Pb adsorbed on kaolinite increased, while the amount of Pb adsorbed on humic acid and ferrihydrites reduced. Netherway et al. (2019) also reported that with the addition of P-rich biochar, increased amounts of Pb-phosphate and pyromorphite with higher stability were found compared with the control soil. A three-year paddy field study showed that wheat straw-derived biochar significantly increased the alkalinity and total organic carbon with a reduction of extractable Pb (Bian et al., 2014).

The surface oxygen-containing functional groups and minerals in nano-structure of the biochar and/or biomass are responsible for the immobilization of PTEs (Joseph et al., 2013; Xu et al., 2017). They are also sensitive to the variation of E_h and may further influence the immobilization effects. The oxygen-containing functional groups are essential factors in the redox-related reactions as a buffer responding to the variation of E_h (Yuan et al., 2017). For example, phenolic species (hydroquinone) act as electron donating moieties while quinones and polycondensed aromatic structures accept electrons and act as redox buffers (Klüpfel et al., 2014). The redox feature of biochar caused by the quinones and polycondensed aromatic structures are strongly affected by the heating temperatures and feedstocks (Klüpfel et al., 2014). Besides, the setup of pyrolysis systems, feedstock preparation, heating rate, supply of oxygen, and retention time in the heating process are also considered as the crucial factors for the redox properties of biochar (Cantrell et al., 2012; Klüpfel et al., 2014).

As a result, variation of E_h can influence the immobilization effects of PTEs by biochars. For instance, the dissolved phases of Cd, Cu, Ni, and Zn in a paddy soil amended by rice hull biochar were increased under oxic conditions, (El-Naggar et al., 2018). Nevertheless, the Pb phytoavailability was slightly higher under oxic (200–250 mV) compared to reducing conditions (Beiyuan et al., 2017a). However, the mechanisms of Pb immobilization/dissolution by biochar under changeable redox conditions and the associated speciation changes of Pb in soil were still not fully clear.

Therefore, we aimed to evaluate the variation of the immobilization effects of soluble Pb by biochar produced at two different temperatures (300 and 550 °C) and its feedstock (pine sawdust biomass) under dynamic E_h conditions (from −300 to +250 mV). Key field-relevant environmental features of soil-solution system without or with different amendments under such dynamic E_h conditions were scrutinized to further understand the behaviors of Pb. The XAFS (X-ray absorption fine structure) spectroscopy was also applied to elucidate the speciation of Pb in soil samples under different treatments and E_h conditions. These can advance our understanding of the underlying mechanisms on biochar immobilization and proper application of biochar for Pb-contaminated soils under flooding conditions.

2. Materials and methods

2.1. Soil and soil amendments

Soil samples were collected from an upper soil layer (0–40 cm) of an agricultural field which is close to a mine (Tancheon) in Gongju city, Republic of Korea, thereafter, air-dried, removed debris, and sieved (< 2 mm). The Tancheon mine was a gold mine, which was opened for many years and closed in 2008. The soil texture of the collected samples is sandy loam, according to our previous study (Igalavithana, et al., 2017). Total contents of As and Pb (2047 and 1680 mg kg^{-1}) were determined in soil according to a measurement by inductively coupled plasma optical emission spectrometry (ICP-OES, Horiba, Germany) after acid digestion (USEPA, 1994). The feedstock of biochar, pine sawdust biomass (BM), was collected from a sawmill company in Seoul, Republic of Korea, air-dried after pre-washing by deionized water, and sieved (< 1 mm). Two temperatures of biochar production were selected, 300 and 550 °C; and the products were named BC300 and BC550. A detailed pyrolysis procedure of the biochar was documented in Lou et al. (2016a,b).

2.2. Pre-incubation experiment

The pre-incubation was conducted at 70% soil water holding capacity and 25 °C for a period of 105 days to have an ageing effect. The BM, BC300, and BC550 were added into soil at a dosage of 5 wt% (equal to 70 t ha^{-1}) which is commonly used in biochar-amended soil (Moon et al., 2013; El-Naggar et al., 2019a,b; Yang et al., 2018). The soils after incubation are referring as S&BM, S&BC300, and S&BC550, while a control sample (CS) without any amendment was prepared. After pre-incubation, the soil samples (with or without amendments) were air-dried and analyzed their physicochemical properties which are documented in Table S1.

2.3. Experiment under pre-defined redox conditions

After passing through a sieve of 0.15 mm, 210 g of the pre-incubated soil samples of CS, S&BM, S&BC300, and S&B550, respectively, were mixed with 1680 mL tap water into one biogeochemical microcosm system (MC). The intelligent MCs can mimic varying redox conditions and automatically record pH and E_h values every 10 min. More technical details were documented by Yu and Rinklebe (2011). At the beginning of the experiment, the slurry was flushed with N_2 to reach the lowest E_h. Additionally, carbon sources for soil microorganisms, i.e. wheat straw (15 g) and glucose (5 g), were added into MCs at the beginning of experiment to reduce the E_h by activating the microorganic activities to reduce the E_h as low as possible. Each amendment had four

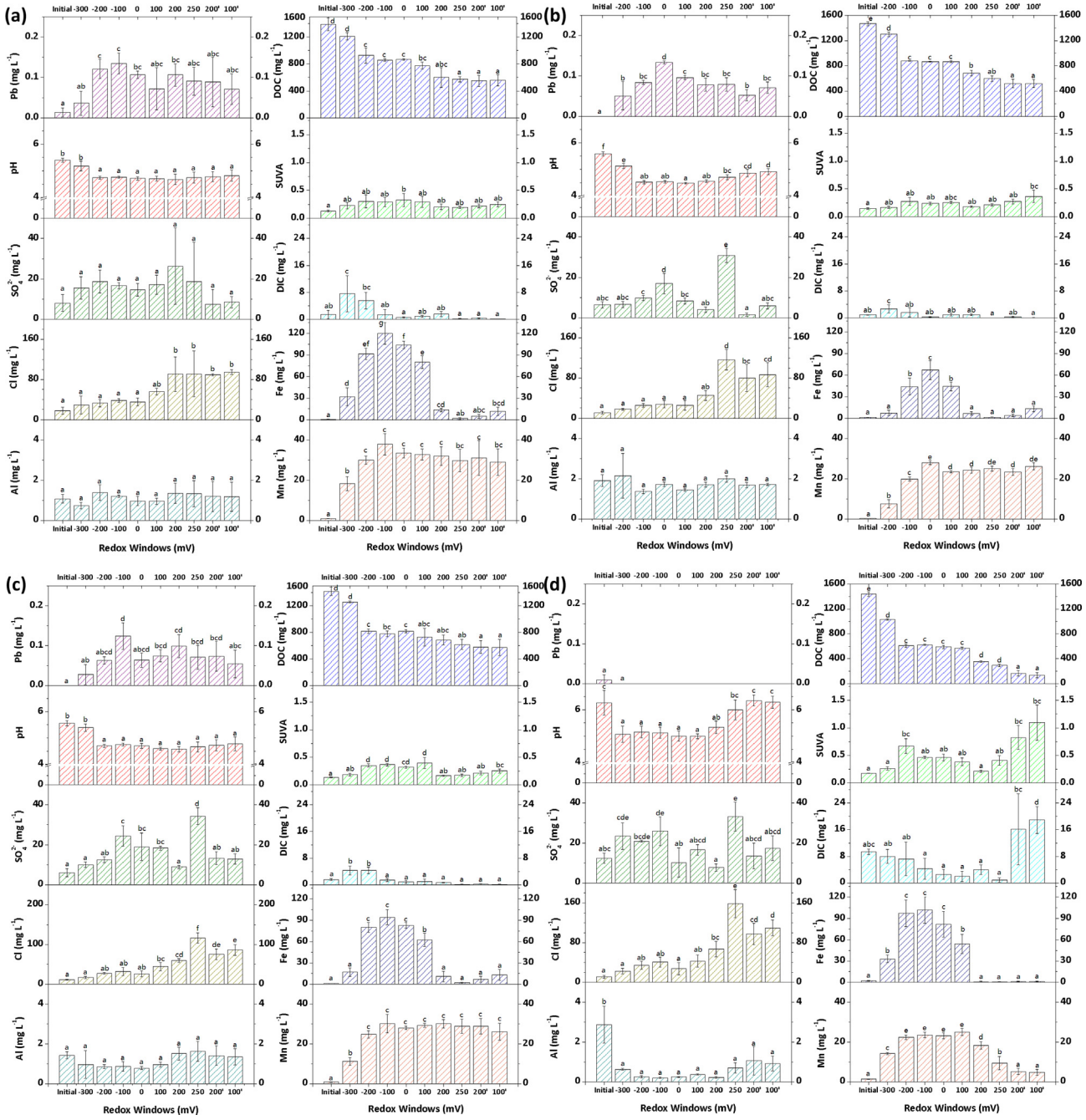

Fig. 1. Influence of dynamic redox conditions (E_h) on the variation of dissolved Pb, pH, sulfate (SO_4^{2-}), chloride (Cl^-), dissolved organic carbon (DOC), SUVA, dissolved inorganic carbon (DIC), dissolved Fe, Mn, and Al in (a) a contaminated soil (CS), the contaminated soil amended with (b) pine sawdust biomass (S&BM), (c) pine sawdust biochar produced at 300 °C (S&BC300), and (d) biochar produced at 550 °C (S&BC550). The same letters above the bars indicate that the results are not significantly different according to the Tukey's test ($p < 0.05$).

independent replications; therefore, the total number of the MCs was 16. Ten pre-defined redox windows, from −300 to +250 mV (initial, −300, −200, −100, 0, 100, 200, 250, 200′, and 100′ mV), were obtained by flushing the slurry with synthetic air or O_2 to gradually increase the E_h. These redox windows were selected based on a preliminary experiment to study the possible redox conditions which might be varied due to the soil properties. The lowest E_h values were approximately −300 mV for the CS, S&BC300, S&BC550, yet the E_h can only reach around −200 mV as minimum for BM. Detailed E_h conditions (maximum, minimum, and average) have been documented in Beiyuan et al. (2017a).

After 1-h mixing of CS, S&BM, S&BC300, and S&BC550 in MCs, the initial sampling was conducted. For selected redox windows, after the adjustment of E_h, a 24-h maintenance by purging synthetic air or O_2 to the system was performed before sampling to have a better mixing of the slurry. An approximately 70 mL of slurry sample was collected for every MC, immediately centrifuged at 5000 rpm for 15 min, and transferred to an anaerobic glovebox (Don Whitley Scientific, Shipley, UK) to separate liquid and solid phases by 0.45-μm filter membranes (Whatman Inc., Maidstone, UK). The glove box was purged by a gas mixture (5% H_2 and 95% N_2) to control the oxygen concentration inside within 0–0.1% (as anoxic conditions). After centrifugation, the filtered supernatant was further separated to liquid sub-samples for different analysis (metal(loid)s, total carbon (TC), DOC, dissolve inorganic

matter (DIC), total nitrogen (TN), and anion groups), and stored in refrigerators at 4 °C.

2.4. Analysis methods for metal, DOC, DIC, TN, and inorganic groups

The liquid sub-samples for metal analysis were firstly prepared by adding concentrated nitric acid (HNO_3) at a volumetric ratio of 1% (v/v), and subsequently detected by ICP-OES. Total carbon, DOC, DIC, and TN in the liquid samples were determined by a C/N-analyzer (Analytik Jena, Germany). The specific ultraviolet absorbance (SUVA) values were obtained by dividing the UV absorbance (at 254 nm) of liquid samples with their DOC concentration (Weishaar et al., 2003). Concentrations of anion groups, such as nitrite (NO_2^-), nitrate (NO_3^-), sulfate (SO_4^{2-}), chloride (Cl^-), and phosphate (PO_4^{3-}), were measured by an ion chromatograph (Metrohm, Germany).

2.5. XAFS study for Pb speciation after pre-incubation in soil

Lead L_{III}-edge XAFS measurements were performed at the BL07A beamline in the National Synchrotron Radiation Research Center (NSRRC) in Taiwan. The wet soil samples collected under different redox conditions and treatments were sealed and prepared in acrylic holders in 2-mm thickness by Kapton tape to avoid desiccation and oxidation in an O_2-free glove box. The samples were stored in a zip bag from which air was removed. Thereafter, the zip bags were stored in a freeze box which was filled with dry ice, and transferred to NSRRC directly. A number of Pb-containing reference standards were included, such as Pb adsorbed on humic acid, PbS, $PbCO_3$, PbO, PbO_2, $PbSiO_3$, $Pb_3(PO_4)_2$, $Pb(CH_3COO)_2$, and $Pb(OH)_2$. The XAFS data were processed using the Athena 0.9.25 package (Ravel and Newville, 2005). Solid samples by different amendments were analysed by linear combination fitting (LCF) which was conducted on the X-ray absorption near-edge structure (XANES) data (Kameda et al., 2017; Li et al., 2016a). The best LCF result we obtained was used in this study, after trying all the binary combinations of the reference materials. Table S2 shows the computed proportions of Pb speciation of the best LCF results. The details of XANES analysis in NSRRC and LCF were documented in Supplementary Information (SI).

2.6. Statistical analysis

Average of the replicated data collected from the MCs were present for 6 h prior to sampling were calculated and used. The significance levels ($p < 0.05$) for each treatment in Fig. 1 were analyzed by Tukey's multiple range tests. Pearson's correlation analysis and factor analysis among Pb and other environmental factors of E_h, pH, DOC, DIC, SUVA, Cl^-, SO_4^{2-}, Al, Fe, Mn, and S were conducted by IBM SPSS Statistics version 22.0.

To study the connections among the key features and complex cause-and-effect interaction of the solubility of Pb in the systems of CS and amended with BM and biochar, factor extraction by Principal Component Analysis for factor analysis was performed. We aim to identify the linkage of factors (i.e. E_h, pH, DOC, DIC, SUVA, Cl^-, SO_4^{2-}, Al, Fe, and Mn) which are thought to have an effect on Pb behavior. Also, cause-and-effect interrelationships among the measured factors under dynamic E_h conditions should be identified. The Varimax-rotation procedure of the factor analysis, with a limited interaction calculation number of 25, was selected. Canonical discriminant analysis (CDA) was also conducted of all analyzed factors in Section 2.4 by SPSS to determine the differentiation among groups (untreated soil and the soil amended with BM, BC300, and BC550) (Shaheen et al., 2017).

3. Results and discussion

3.1. Variation of pH, DOC, DIC, SUVA, Al, Fe, Mn, and anion groups under dynamic E_h conditions with interactions by biomass and biochar

The soil pH of CS (i.e., without the amendments) ranged from 4.5 to 5.5 under various redox windows (Fig. 1a). The soil pH was greatly reduced from 5.5 to 4.7 after the second sampling (the lowest redox window: −300 mV) with the start of purging oxygen-containing synthetic air to increase the E_h. This might be due to the CO_2 and organic acids generated from the degradation of organic matter by microbial activities under anoxic conditions (Rinklebe and Shaheen, 2017; Shaheen et al., 2014; Wang et al., 2012). By contrast, negative relationships of soil pH and E_h were commonly reported, which was associated with the demand of anoxic protons for reducing NO_3^-, Mn (VI), and Fe(III) (Frohne et al., 2014; Frohne et al., 2011).

The pH of the soil slurry ranged from 5.0 to 6.7 in the case of S&BC550 under various E_h conditions, while the pH stayed in the range of 4.5 to 5.5 in the cases of S&BM and S&BC300, respectively. This could be attributed to the higher alkalinity of BC550 (7.4), although the pH values of BM (5.1) and BC300 (5.9) were only slightly higher than the soil pH (4.2) (Beiyuan et al., 2017a). The pH variation pattern of S&BC550 differentiated from the other three systems, i.e., the pH increased after purging oxygen/synthetic gases.

The pH of the slurry system of S&BC550 boosted sharply in the E_h windows of +100 to 250 mV and reached at a peak of 6.7 at the 200′ mV E_h window, which was even higher than the pH at the beginning of the experiment (Fig. 1d). This might be associated with the redox reactions of BC550. Biochar originates from the same feedstock but produced at intermediate temperature (400–500 °C) have higher quinone moieties than those produced at low temperature (< 400 °C) (Klüpfel et al., 2014). In our case, there could be more quinone moieties, which can act as major electron acceptors, generated from the BC550 than BC300 and BM. The increase of pH starting at the +200 mV E_h window was probably because the quinone moieties were reduced to hydroquinone under oxic conditions with consumptions of H^+.

The concentration of dissolved Fe of CS was significantly higher under anoxic conditions (< +100 mV) than oxic conditions (> +100 mV), especially in the redox windows of −200 to 100 mV (Fig. 1a). The results were strongly associated with the redox chemistry of Fe oxides (Fe(II)/Fe(III)). Iron oxides can be dissolved as Fe(II) under anoxic conditions, while Fe presumably re-crystallized as oxides under oxic conditions (Takeno, 2005). However, large amounts of dissolved Fe were reduced starting at 200 mV, though the slurry pH was acidic. The phenomenon was not fully consistent with the E_h-pH diagrams (Takeno, 2005). This might be due to additional interactions with the aromatic dissolved organic matter (DOM, indicated by SUVA in this study), Mn^{2+}, Pb^{2+}, and Cl^-, according to the results of Pearson's correlation analyses (Table S3). The concentration of dissolved Fe was suppressed by the amendments with an order of BM > BC300 > BC550 (Fig. 1). The dissolution pattern of Fe under different redox windows are similar for all four soil-slurry systems. The Pearson's correlation analyses suggested that Fe had strong connections between pH and E_h ($p < 0.01$) for BM, SUVA, E_h, Al, and Cl for BC300, and Mn, pH, E_h, Cl, Al, and TN for BC550 (Table S3-6).

The Mn mostly existed in a dissolved form under various E_h conditions (from −270 to +250 mV) due to the acidic conditions of CS (Fig. 1a) (Mn(II)/Mn(IV)). Higher concentrations of Mn were observed under oxic conditions. This result was consistent with the Mn E_h-pH diagram (Takeno, 2005). The amount of dissolved Mn was significantly limited by the amendment of BC550, especially under oxic conditions (from redox windows of 200 to 100′ mV, Fig. 1d), while it was slightly inhibited by the addition of BM and BC300. This phenomenon might be associated with the increase of pH by the amendments. Also, the Pearson's correlation analyses supported that the Mn concentration was strongly related to pH, DOC, and Fe (Table S3-6).

Table 1
Pearson's correlation relation among Pb and environmental factors (E_h, pH, DOC, SUVA, Fe, Mn, Al, DIN, Cl, and Sulphate) in the control contaminated soil (CS), the contaminated soil amended with pine sawdust biomass (S&BM), pine sawdust biochar produced at 300 °C (S&BC300), and biochar produced at 550 °C (S&BC550) (n = 40).

	pH	Pb	DOC	SUVA	Fe	Mn	Al	DIC	Cl	Sulphate
CS										
E_h	n.s.	n.s.	−0.315*	−0.412**	−0.628**	n.s.	n.s.	−0.640**	0.464**	n.s.
pH	1	−0.781**	0.684**	−0.378*	−0.343*	−0.858**	−0.403**	n.s.	−0.420**	n.s.
Pb		1	−0.391*	n.s.	0.470**	0.788**	0.588**	n.s.	n.s.	0.423**
S&BM										
E_h	n.s.	n.s.	n.s.	n.s.	−0.433**	n.s.	n.s.	−0.594**	0.449**	n.s.
pH	1	−0.845**	0.605**	n.s.	−0.572**	−0.838**	0.374*	n.s.	n.s.	n.s.
Pb		1	−0.455**	n.s.	0.688**	0.772**	n.s.	n.s.	n.s.	n.s.
S&BC300										
E_h	n.s.	n.s.	n.s.	−0.414**	−0.574**	n.s.	0.571**	−0.783**	0.531**	n.s.
pH	1	−0.755**	0.784**	−0.402*	−0.364*	−0.941**	n.s.	0.365*	−0.517**	−0.483**
Pb		1	−0.505**	0.331*	0.406**	0.791**	n.s.	n.s.	n.s.	0.423**
S&BC550										
E_h	0.565**	n.s.	n.s.	n.s.	−0.640**	−0.449**	0.353*	n.s.	0.489**	n.s.
pH	1	0.379*	n.s.	0.373*	−0.644**	−0.852**	0.561**	0.564**	0.467**	n.s.
Pb		1	n.s.	n.s.	−0.387*	−0.422**	0.517**	n.s.	n.s.	n.s.

n.s. non-significant.
* $p < 0.05$.
** $p < 0.01$.

The DOC decreased after purging with O_2, which could be associated with the addition of O_2 for aerobic microbes to consume the DOC and reduce the high E_h at the initial redox window (Fig. 1). In general, opposite performance of E_h and DOC was found, which corroborated that complex organic matter can be decomposed to DOC through reductive hydrolysis in anoxic environment (Frohne et al., 2014; Husson, 2013; Yu et al., 2007). The DOC was significantly associated with Cl^-, TN, pH, Mn and S, according to the results of Pearson's correlation analyses for CS. Unexpectedly, the addition of BM and BC300 only caused negligible effects on DOC, i.e., the variation of DOC of CS, S&BM, and S&BC300 were similar (Fig. 1). The amount of DOC was greatly reduced by adding BC550, in comparison with other scenarios, especially under oxic conditions (from +200 mV to +100′ mV windows).

The initial concentration of SO_4^{2-} in CS was the lowest after the 1-h initial mixing under oxic conditions (SO_4^{2-}/S^{2-}). The sulfate concentration increased after reaching the lowest E_h condition (−300 mV redox window), and it gradually increased with rising the E_h until reaching the maximum E_h. The variation pattern of SO_4^{2-} can be affected by the variation of DOC and pH (Rinklebe et al., 2016a). The addition of amendments slightly increased SO_4^{2-} which was probably associated with the change of DOC and pH by adding the biomass and biochar in the present study.

3.2. Dynamics of Pb under various soil E_h conditions with interactions by biomass and biochar

The dissolved Pb concentration of CS was in the range of 0.01–0.17 mg L^{-1} under various examined E_h windows (Fig. 1a). The dissolved Pb was remarkably reduced by the addition of BC550 (under 0.01 mg L^{-1} for all E_h windows, Fig. 1d), while it was slightly reduced by the amendment of BM and BC300 to the ranges of 0–0.13 and 0–0.12 mg L^{-1}, respectively (Fig. 1b & c). A similar trend of Pb phytoavailability was observed in our previous study (Beiyuan et al., 2017a). The intensive reduction on dissolved Pb can probably be related to the higher alkalinity of BC550 (pH = 7.4) compared to BM (pH = 5.1) and BC300 (pH = 5.9). The mobility of Pb can be significantly affected by pH as the solubility of Pb was reduced with an increasing pH (Dong et al., 2000). Significant change of pH was found with the assistance of BC550 as discussed in the previous section, which presumably is one of reasons leading to the Pb immobilization, which is consistent with previous finding (Ahmad et al., 2012; Ahmad et al., 2014a; Shen et al., 2019a,b). The enrichment of alkalinity by BC550 increased negative charge of the soil surface, which might also lead to higher adsorption affinity of Pb (Ahmad et al., 2014b).

The immobilization effect caused by oxygen-containing functional groups was not obvious in comparison with the alkalinity in this study, though biochar with high oxygen-containing functional groups is expected to be able to effectively immobilize metals, especially for soft Lewis acids such as Pb^{2+} (Ahmad et al., 2016c; Uchimiya et al., 2011). Marginal difference on the dissolved Pb caused by the addition of BM and BC300 was found, despite BM has a higher O/C ratio (BM = 0.66 and BC300 = 0.33) resulted in reduced oxygen-containing functional groups followed the increased pyrolysis temperatures (Awad et al., 2018).

The amount of dissolved Pb reached the highest under slightly anoxic conditions (at the redox windows of −100 to 0 mV) with or without the addition of BM and BC300. This might be mainly attributed to the dissolution of Fe/Mn oxides under reducing conditions which thereafter lead to a release of co-precipitated and adsorbed Pb (Du Laing et al., 2009b). This can be further supported by the fact that higher amounts of dissolved Fe and Mn (more obviously for Fe) were found at similar E_h windows (−100 to 0 mV, Fig. 1). In addition, the geochemical fractionation results indicated that Pb in the soil was mainly bound to the residue, crystalline iron oxide, and carbonated fractions (Beiyuan et al., 2017a).

A decreasing trend of dissolved Pb started at −100 mV to 100 mV for all cases (except S&BC550), which might be associated with the formation of Fe/Mn oxides. These generated Fe/Mn oxides have a higher cation exchange capacity and surface area which are favorable for the adsorption of Pb ions (Antic-Mladenovic et al., 2017). In addition, the results of Pearson's correlation analysis further supported that Mn, pH, Al, Fe, and SO_4^{2-} were the most significant features influencing the amount of soluble Pb in the four scenarios ($p < 0.01$) (Table 1), whereas DOC and SUVA also played important roles in controlling the solubility of Pb ($p < 0.05$).

3.3. Speciation of Pb in soil phase by XANES analysis

Fig. 2 shows the LCF results of Pb XANES spectra of soil samples collected from both anoxic (the lowest E_h) and oxic conditions (the highest E_h) of all four scenarios, respectively. The results indicated that

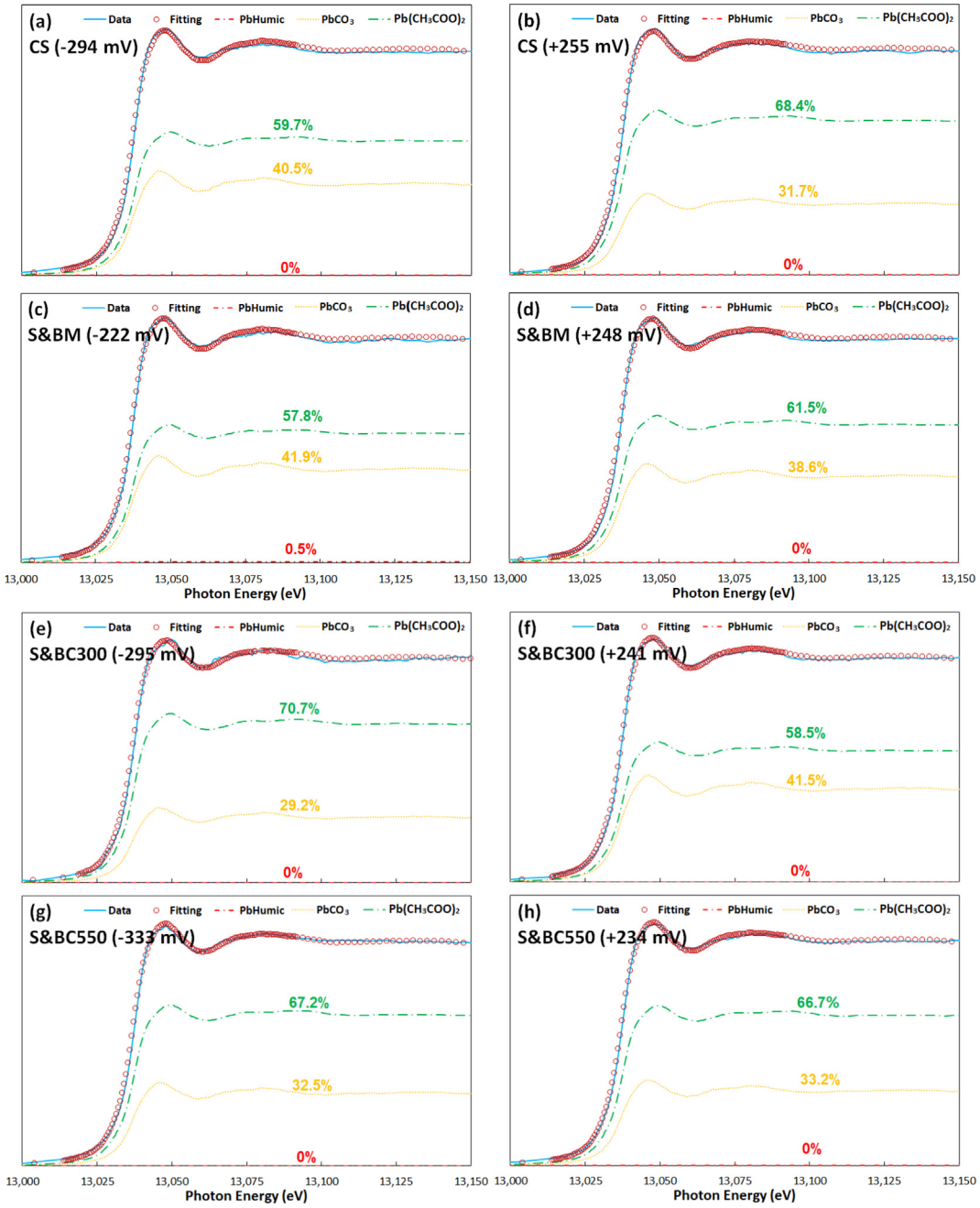

Fig. 2. Linear combination fitting of Pb-XANES results of a contaminated soil (CS), the contaminated soil amended with pine sawdust biomass (S&BM), pine sawdust biochar produced at 300 °C (S&BC300), and biochar produced at 550 °C (S&BC550) under anoxic ((a) CS; (c) S&BM; (e) S&BC300; and (g) S&BC550) and oxic conditions ((b) CS; (d) S&BM; (f) S&BC300; and (h) S&BC550).

the speciation of Pb changed from an anoxic to oxic condition, which was mainly contributed to $Pb(CH_3COO)_2$ and $PbCO_3$. The results showed a decrease of the proportion of $PbCO_3$ for CS (Fig. 2a & b) and S&BM (Fig. 2c & d). It is possible that the decrease of $PbCO_3$ in CS and S&BM was mainly caused by the reduction of pH instead of an increased amount of $Pb(CH_3COO)_2$. $PbCO_3$ is a stable compound with low solubility ($K_{sp}(PbCO_3) = 7.45 \times 10^{-14}$). However, the decreasing pH can lead to enhanced hydrolysis of CO_3^{2-} to HCO_3^- and H_2CO_3, which reduce the amount of $PbCO_3$ and increases the amount of Pb^{2+}. A decrease of pH (from ~5.5 to 4.8 and 5.0 to 4.5, respectively, for CS and S&BM) with a growing amount of free Pb^{2+} ions were observed that under the same E_h conditions (−300 and 250 mV, respectively; Fig. 1). Besides, organic matter can become less electronegative caused by the reduction of alkalinity under oxic conditions (Grybos et al., 2007), which could lead to a decreasing amount of Pb adsorbed on humic acid. However, the variation of the proportion of Pb adsorbed on humic acid was not obvious for all analyzed samples based on our LCF results.

Unlike S&BM, an obvious increase in the proportion of $PbCO_3$ was found for S&BC300 (Fig. 2e & f); however, the solubility of $PbCO_3$ is expected to increase under such a decrease of pH from ~5.5 to 4.8. In addition, an increased amount of dissolved Pb of S&BC300 was observed from anoxic to oxic conditions (Fig. 1). This might suggest a significant decreasing amount of $Pb(CH_3COO)_2$ which probably lead to increasing Pb mobility, leachability, and availability. Though a similar immobilization effect on Pb caused by the rich oxygen-containing functional groups on the surface of BM and BC300 was suggested, the functional groups after pyrolysis (i.e., BC300) are presumably more sensitive to the variations of E_h. With a pyrolysis temperature range of

200 to 350 °C, functional groups like the carboxyl C═O, aromatic C═C, and C═O of conjugated ketones and quinones are generated/increased (Uchimiya et al., 2011). This suggested that biochar produced at 300 °C contains higher amounts of carboxyl groups which can contribute to Pb immobilization. Besides, some of the functional groups are redox-sensitive (can be act as electronic donor or acceptor and therefore affecting their Pb immobilization capacity), specially for carboxyl groups in this study (Klüpfel et al., 2014; Yuan et al., 2017). These contributed to the different redox behaviors of BM and BC300, even though they have similar immobilization effects without affecting by E_h. In addition, the change of pH caused by BM should be considered.

Subtle changes of Pb speciation were observed under varied redox conditions for S&BC550 (Fig. 2g & h), which might be attributed to the high alkalinity of BC550. This further proves our hypothesis that the pyrolysis process under higher temperatures makes the organic amendment more stable and resistant in a redox-sensitive environment.

3.4. Principle component analysis and canonical discriminant analysis statistical analysis

The statistical results supported that the system was complex and the factors (i.e. E_h, pH, DOC, DIC, SUVA, Cl^-, SO_4^{2-}, Al, Fe, and Mn) were strongly influenced by each other. Two controlling components are presented in Fig. 3. The total explained variance of the two top components in CS is 64.19% (37.70% Component 1 and 26.49% Component 2), in S&BM is 68.88% (42.89% Component 1 and 25.67% Component 2), in S&BC300 is 73.54% (41.94% Component 1 and 31.60% Component 2), and in S&BC550 is 61.63% (38.62% Component 1 and 23.00% Component 2). More than two components were achieved in the factor analysis of the four different systems, i.e., a complex system was established under flooding conditions.

The results of factor analysis in CS suggest that the dissolved Pb was rather associated with Mn than other factors, which indicates similar geochemical behaviors of dissolved Pb and Mn under the pre-set variable E_h windows (Fig. 3a), which is consistent with the dissolved concentration of Pb and Mn (Fig. 1a). The result is consistent with previous studies which suggested a higher affinity of Pb to Mn oxides than Fe oxides (up to 40 times) (Rinklebe et al., 2016b). By contrast, the behavior of Fe was largely associated with SUVA (Fig. 3a). In addition, the results also support that the most significant factors for Component 1 were pH, Pb, and Mn followed by DOC, while E_h and Fe were the most crucial elements followed by Cl, SUVA, and DIC (Table S7).

With the amendment of BM, the dissolved Pb was relatively associated with mineral elements such as Mn and Fe more than other features in this system (Fig. 3b), which differed from the results of CS. By contrast, the change of S&BC300 was smaller compared with CS. After incubation with BC300, the release pattern of the dissolved Pb in soils was relatively similar to Mn and sulfate, while the behavior of dissolved Fe was relatively linked to SUVA. The factor analysis results also suggest that dissolved Pb of S&BM and S&BC300 mainly contributed to

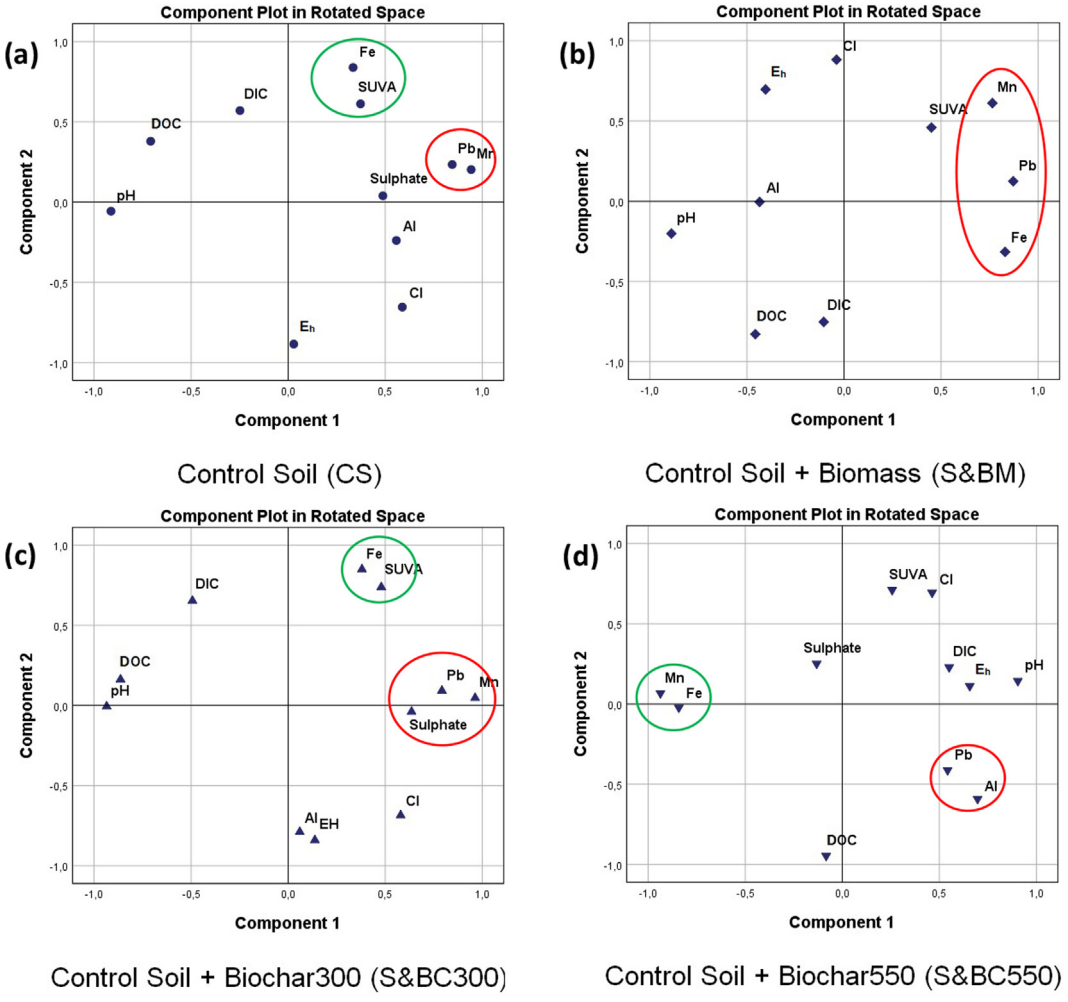

Fig. 3. Factor analysis of dissolved Pb, E_h, pH, sulfate (SO_4^{2-}), chloride (Cl^-), dissolved organic carbon (DOC), SUVA, dissolved inorganic carbon (DIC), dissolved Fe, Mn, and Al in (a) a contaminated soil (CS), (b) the contaminated soil amended with pine sawdust biomass (S&BM), (c) amended with pine sawdust biochar produced at 300 °C (S&BC300), and (d) biochar produced at 550 °C (S&BC550).

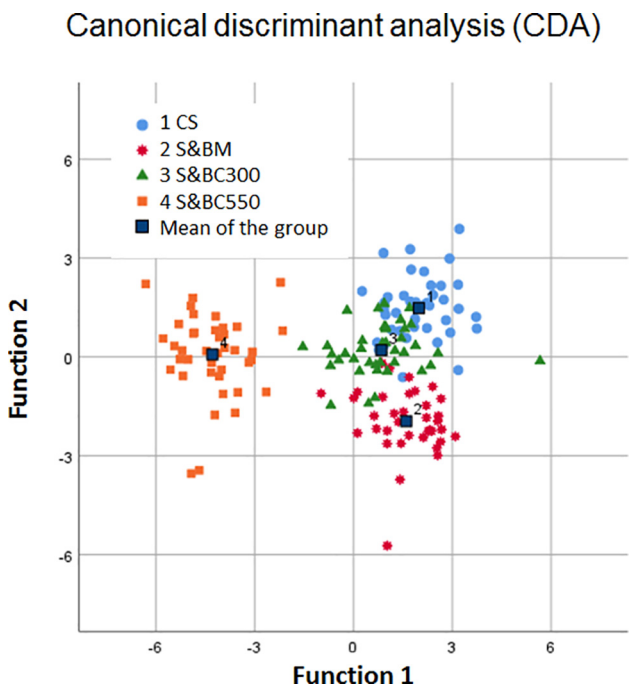

Fig. 4. Canonical discriminant analysis of dissolved Pb, E_h, pH, sulfate (SO_4^{2-}), chloride (Cl^-), dissolved organic carbon (DOC), SUVA, dissolved inorganic carbon (DIC), dissolved Fe, Mn, and Al in a contaminated soil (CS), the contaminated soil amended with pine sawdust biomass (S&BM), amended with pine sawdust biochar produced at 300 °C (S&BC300), and biochar produced at 550 °C (S&BC550).

Component 1 including pH, Mn, and organic components (DOC and DIC), while the Component 2 included Fe and E_h (Table S7). However, for S&BC550, dissolved Pb contributed to Component 1 and 2 almost equally, where Component 1 mainly contained pH, Fe, and Mn and Component 2 included DOC, SUVA, and Al (Table S7). The results could further indicate that the mechanism of influencing the behaviors of Pb by BM and BC300 were different, which is consistent with our previous XANES analysis results. Secondly, the behavior of Pb was affected by BC550 and differ significantly from the CS and BC300, while Pb was completely immobilized by BC550 under various E_h conditions.

The results of the canonical discriminant analysis (CDA) in Fig. 4 illustrate that CS, S&BM, S&BC300, and S&BC550 could be clearly discriminated. This means that the geochemical behavior of the release of Pb and the controlling factors are significantly different due to the different treatments. The S&BC550 showed significantly a different behavior from CS, S&BM, and S&BC300, as only a small overlap was found including all dissolved analytical data. Overall, the similarity of CS and S&BC300 was higher than CS and S&BM according to some overlaps. A slight overlay also existed between S&BM and S&BC300. Function 1 can contribute to 69.4% of variability of the four types of soils, while function 2 was able to explain 29.2%. Function 1 discriminated the soils into two groups: 1) CS, S&BM, and S&BC300, and 2) S&BC550; whereas function 2 discriminated the soils into two groups of 1) CS, S&BC300, and S&BC550, and 2) S&BM. The higher discrimination was found based on function 1.

Standardized canonical discrimination coefficients (listed in Table S8) results indicated that DOC, Pb, Cl, Fe, and SO_4^{2-} were able to explain the discrimination of the samples according to function 1, while Mn, pH, TN, Al, and DOC were able to explain the discrimination based on function 2. The major difference between S&BC550 and the other three systems was in the features of DOC, Pb, Cl, Fe, and SO_4^{2-}. Those finding demonstrated that the application of BC550 significantly altered the Pb behavior and contributed to its Pb immobilization effects.

4. Conclusions

The dissolved Pb from the contaminated soil was almost completely hampered by the application of BC550, while it was limitedly immobilized by BM and BC300. The Pb immobilization by all amendments was significantly affected by the variation of E_h. In summary, the possible mechanisms of the dynamic E_h on affecting the Pb immobilization effects by BM, BC300, and BC550 are: (1) influences on the release and resorption of soil dissolved Pb by altering the redox chemistries of pH, Fe, Mn, Al, DOC, SUVA, and S and (2) influences on the Pb immobilization effects by complexation of the functional groups and precipitation. Our XANES results also suggested that biochar produced at higher temperatures can be more suitable for immobilization of Pb under dynamic E_h conditions, and it is more stable and reluctant to the variation of E_h. Further investigations on the detailed change of functional groups caused by the dynamic E_h are needed, especially for those are responsible for Pb immobilization. Given the significant implication of Pb, future studies on other PTEs-contaminated paddy soils amended by biochar should be conducted, especially for redox-sensitive PTEs. Also, the gained results should be verified under field conditions in future. This can contribute to the application of biochar in contaminated paddy soils for rice which is popular in Asian countries.

CRediT authorship contribution statement

Jingzi Beiyuan: Writing - original draft, Visualization, Investigation, Formal analysis. **Yasser M. Awad:** Investigation. **Felix Beckers:** Investigation. **Jianxu Wang:** Formal analysis. **Daniel C.W. Tsang:** Resources, Writing - review & editing, Conceptualization. **Yong Sik Ok:** Resources, Writing - review & editing, Conceptualization, Funding acquisition. **Shan-Li Wang:** Resources, Formal analysis. **Hailong Wang:** Resources. **Jörg Rinklebe:** Supervision, Conceptualization, Methodology, Writing - review & editing, Resources.

Declaration of Competing Interest

The authors declared that there is no conflict of interest.

Acknowledgments

The authors appreciate the financial support by the National Research Foundation of Korea (NRF-2015R1A2A2A11001432), a Korean University Grant, the National Natural Science Foundation of China (21577131, 21876027), and the Natural Science Foundation of Guangdong Province, China (2017A030311019). We are grateful to the National Synchrotron Radiation Research Center, Taiwan, for the valuable beamtime and the support. The authors thank Mr. C. Vandenhirtz and Mr. Jan Schneider of University of Wuppertal for their technical and experimental assistance. The authors also appreciate Ms Puu-Tai Yang of National Taiwan University for her kind help on Pb XANES analysis.

Appendix A. Supplementary material

Supplementary data to this article can be found online at https://doi.org/10.1016/j.envint.2019.105376.

References

Ahmad, M., Hashimoto, Y., Moon, D.H., Lee, S.S., Ok, Y.S., 2012. Immobilization of lead in a Korean military shooting range soil using eggshell waste: an integrated mechanistic approach. J. Hazard. Mater. 209–210, 392–401.

Ahmad, M., Lee, S.S., Lee, S.E., Al-Wabel, M.I., Tsang, D.C.W., Ok, Y.S., 2016a. Biochar-induced changes in soil properties affected immobilization/mobilization of metals/metalloids in contaminated soils. J. Soil. Sediment.

Ahmad, M., Lee, S.S., Lim, J.E., Lee, S.E., Cho, J.S., Moon, D.H., Hashimoto, Y., Ok, Y.S., 2014a. Speciation and phytoavailability of lead and antimony in a small arms range

soil amended with mussel shell, cow bone and biochar: EXAFS spectroscopy and chemical extractions. Chemosphere 95, 433–441.
Ahmad, M., Ok, Y.S., Kim, B.Y., Ahn, J.H., Lee, Y.H., Zhang, M., Moon, D.H., Al-Wabel, M.I., Lee, S.S., 2016b. Impact of soybean stover- and pine needle-derived biochars on Pb and As mobility, microbial community, and carbon stability in a contaminated agricultural soil. J. Environ. Manage. 166, 131–139.
Ahmad, M., Ok, Y.S., Rajapaksha, A.U., Lim, J.E., Kim, B.Y., Ahn, J.H., Lee, Y.H., Al-Wabel, M.I., Lee, S.E., Lee, S.S., 2016c. Lead and copper immobilization in a shooting range soil using soybean stover- and pine needle-derived biochars: chemical, microbial and spectroscopic assessments. J. Hazard. Mater. 301, 179–186.
Ahmad, M., Rajapaksha, A.U., Lim, J.E., Zhang, M., Bolan, N., Mohan, D., Vithanage, M., Lee, S.S., Ok, Y.S., 2014b. Biochar as a sorbent for contaminant management in soil and water: a review. Chemosphere 99, 19–33.
Antic-Mladenovic, S., Frohne, T., Kresovic, M., Stark, H.J., Tomic, Z., Licina, V., Rinklebe, J., 2017. Biogeochemistry of Ni and Pb in a periodically flooded arable soil: fractionation and redox-induced (im)mobilization. J. Environ. Manage. 186, 141–150.
Antoniadis, V., Levizou, E., Shaheen, S.M., Ok, Y.S., Sebastian, A., Baum, C., Prasad, M.N.V., Wenzel, W.W., Rinklebe, J., 2017. Trace elements in the soil-plant interface: phytoavailability, translocation, and phytoremediation – a review. Earth-Sci. Rev.
Awad, Y.M., Ok, Y.S., Abrigata, J., Beiyuan, J., Beckers, F., Tsang, D.C.W., Rinklebe, J., 2018. Pine sawdust biomass and biochars at different pyrolysis temperatures change soil redox processes. Sci. Total Environ. 625, 147–154.
Beckers, F., Awad, Y.M., Beiyuan, J., Abrigata, J., Mothes, S., Tsang, D.C.W., Ok, Y.S., Rinklebe, J., 2019. Impact of biochar on mobilization, methylation, and ethylation of mercury under dynamic redox conditions in a contaminated floodplain soil. Environ. Int. 127, 276–290.
Beiyuan, J., Awad, Y.M., Beckers, F., Tsang, D.C.W., Ok, Y.S., Rinklebe, J., 2017a. Mobility and phytoavailability of As and Pb in a contaminated soil using pine sawdust biochar under systematic change of redox conditions. Chemosphere 178, 110–118.
Beiyuan, J., Lau, A.Y.T., Tsang, D.C.W., Zhang, W., Kao, C.-M., Baek, K., Ok, Y.S., Li, X.-D., 2018. Chelant-enhanced washing of CCA-contaminated soil: coupled with selective dissolution or soil stabilization. Sci. Total Environ. 612C, 1463–1472.
Beiyuan, J., Tsang, D.C.W., Ok, Y.S., Zhang, W., Yang, X., Baek, K., Li, X.D., 2016. Integrating EDDS-enhanced washing with low-cost stabilization of metal-contaminated soil from an e-waste recycling site. Chemosphere 159, 426–432.
Beiyuan, J., Tsang, D.C.W., Yip, A.C.K., Zhang, W., Ok, Y.S., Li, X.D., 2017b. Risk mitigation by waste-based permeable reactive barriers for groundwater pollution control at e-waste recycling sites. Environ. Geochem. Health 39, 75–88.
Bian, R., Joseph, S., Cui, L., Pan, G., Li, L., Liu, X., Zhang, A., Rutlidge, H., Wong, S., Chia, C., Marjo, C., Gong, B., Munroe, P., Donne, S., 2014. A three-year experiment confirms continuous immobilization of cadmium and lead in contaminated paddy field with biochar amendment. J. Hazard. Mater. 272, 121–128.
Cantrell, K.B., Hunt, P.G., Uchimiya, M., Novak, J.M., Ro, K.S., 2012. Impact of pyrolysis temperature and manure source on physicochemical characteristics of biochar. Bioresour. Technol. 107, 419–428.
Dong, Y., Ma, L.Q., Rhue, R.D., 2000. Relation of enhanced Pb solubility to Fe partitioning in soils. Environ. Pollut. 110, 515–522.
Du Laing, G., Meers, E., Dewispelaere, M., Rinklebe, J., Vandecasteele, B., Verloo, M.G., Tack, F.M.G., 2009a. Effect of water table level on metal mobility at different depths in wetland soils of the Scheldt Estuary (Belgium). Water Air Soil Poll 202, 353–367.
Du Laing, G., Rinklebe, J., Vandecasteele, B., Meers, E., Tack, F.M., 2009b. Trace metal behaviour in estuarine and riverine floodplain soils and sediments: a review. Sci. Total Environ. 407, 3972–3985.
El-Naggar, A., Lee, S.S., Rinklebe, J., Farooq, M., Song, H., Sarmah, A.K., Zimmerman, A.R., Ahmad, M., Shaheen, S.M., Ok, Y.S., 2019a. Biochar application to low fertility soils: a review of current status, and future prospects. Geoderma 337, 536–554.
El-Naggar, A., Shaheen, S.M., Hseu, Z.Y., Wang, S.L., Ok, Y.S., Rinklebe, J., 2019b. Release dynamics of As Co, and Mo in a biochar treated soil under pre-definite redox conditions. Sci. Total Environ. 657, 686–695.
El-Naggar, A., Shaheen, S.M., Ok, Y.S., Rinklebe, J., 2018. Biochar affects the dissolved and colloidal concentrations of Cd, Cu, Ni, and Zn and their phytoavailability and potential mobility in a mining soil under dynamic redox-conditions. Sci. Total Environ. 624, 1059–1071.
Frohne, T., Diaz-Bone, R.A., Du Laing, G., Rinklebe, J., 2015. Impact of systematic change of redox potential on the leaching of Ba, Cr, Sr, and V from a riverine soil into water. J Soil Sediment 15, 623–633.
Frohne, T., Rinklebe, J., Diaz-Bone, R.A., 2014. Contamination of floodplain soils along the Wupper River, Germany, with As Co, Cu, Ni, Sb, and Zn and the impact of pre-definite redox variations on the mobility of these elements. Soil Sediment Contam. 23, 779–799.
Frohne, T., Rinklebe, J., Diaz-Bone, R.A., Du Laing, G., 2011. Controlled variation of redox conditions in a floodplain soil: impact on metal mobilization and biomethylation of arsenic and antimony. Geoderma 160, 414–424.
Grybos, M., Davranche, M., Gruau, G., Petitjean, P., 2007. Is trace metal release in wetland soils controlled by organic matter mobility or Fe-oxyhydroxides reduction? J. Colloid Interface Sci. 314, 490–501.
Husson, O., 2013. Redox potential (Eh) and pH as drivers of soil/plant/microorganism systems: a transdisciplinary overview pointing to integrative opportunities for agronomy. Plant Soil 362, 389–417.
Igalavithana, A.D., Kwon, E.E., Vithanage, M., Rinklebe, J., Moon, D.H., Meers, E., Tsang, D.C.W., Ok, Y.S., 2019. Soil lead immobilization by biochars in short-term laboratory incubation studies. Environ. Int. 127, 190–198.
Igalavithana, A.D., Lee, S.E., Lee, Y.H., Tsang, D.C.W., Rinklebe, J., Kwon, E.E., Ok, Y.S., 2017. Heavy metal immobilization and microbial community abundance by vegetable waste and pine cone biochar of agricultural soils. Chemosphere 174, 593–603.
Jin, J., Li, Y., Zhang, J., Wu, S., Cao, Y., Liang, P., Zhang, J., Wong, M.H., Wang, M., Shan, S., Christie, P., 2016. Influence of pyrolysis temperature on properties and environmental safety of heavy metals in biochars derived from municipal sewage sludge. J. Hazard. Mater. 320, 417–426.
Joseph, S., Graber, E.R., Chia, C., Munroe, P., Donne, S., Thomas, T., Nielsen, S., Marjo, C., Rutlidge, H., Pan, G.X., Li, L., Taylor, P., Rawal, A., Hook, J., 2013. Shifting paradigms: development of high-efficiency biochar fertilizers based on nano-structures and soluble components. Carbon Manag 4, 323–343.
Kameda, K., Hashimoto, Y., Wang, S.L., Hirai, Y., Miyahara, H., 2017. Simultaneous and continuous stabilization of As and Pb in contaminated solution and soil by a ferrihydrite-gypsum sorbent. J. Hazard. Mater. 327, 171–179.
Klüpfel, L., Keiluweit, M., Kleber, M., Sander, M., 2014. Redox properties of plant biomass-derived black carbon (biochar). Environ. Sci. Technol. 48, 5601–5611.
Li, H., Liu, Y., Chen, Y., Wang, S., Wang, M., Xie, T., Wang, G., 2016a. Biochar amendment immobilizes lead in rice paddy soils and reduces its phytoavailability. Sci. Rep. 6, 31616.
Li, H., Ye, X., Geng, Z., Zhou, H., Guo, X., Zhang, Y., Zhao, H., Wang, G., 2016b. The influence of biochar type on long-term stabilization for Cd and Cu in contaminated paddy soils. J. Hazard. Mater. 304, 40–48.
Lou, K., Rajapaksha, A.U., Ok, Y.S., Chang, S.X., 2016a. Pyrolysis temperature and steam activation effects on sorption of phosphate on pine sawdust biochars in aqueous solutions. Chem Spec Bioavailab 28, 42–50.
Lou, K., Rajapaksha, A.U., Ok, Y.S., Chang, S.X., 2016b. Sorption of copper(II) from synthetic oil sands process-affected water (OSPW) by pine sawdust biochars: effects of pyrolysis temperature and steam activation. J Soil Sediment.
Lu, K., Yang, X., Gielen, G., Bolan, N., Ok, Y.S., Niazi, N.K., Xu, S., Yuan, G., Chen, X., Zhang, X., Liu, D., Song, Z., Liu, X., Wang, H., 2017. Effect of bamboo and rice straw biochars on the mobility and redistribution of heavy metals (Cd, Cu, Pb and Zn) in contaminated soil. J. Environ. Manage. 186, 285–292.
Mohan, D., Sarswat, A., Ok, Y.S., Pittman Jr., C.U., 2014. Organic and inorganic contaminants removal from water with biochar, a renewable, low cost and sustainable adsorbent – a critical review. Bioresour. Technol. 160, 191–202.
Moon, D.H., Park, J.W., Chang, Y.Y., Ok, Y.S., Lee, S.S., Ahmad, M., Koutsospyros, A., Park, J.H., Baek, K., 2013. Immobilization of lead in contaminated firing range soil using biochar. Environ. Sci. Pollut. Res. Int. 20, 8464–8471.
Netherway, P., Reichman, S.M., Laidlaw, M., Scheckel, K., Pingitore, N., Gasco, G., Mendez, A., Surapaneni, A., Paz-Ferreiro, J., 2019. Phosphorus-rich biochars can transform lead in an urban contaminated soil. J. Environ. Qual. 48, 1091–1099.
Rajapaksha, A.U., Vithanage, M., Zhang, M., Ahmad, M., Mohan, D., Chang, S.X., Ok, Y.S., 2014. Pyrolysis condition affected sulfamethazine sorption by tea waste biochars. Bioresour. Technol. 166, 303–308.
Ravel, B., Newville, M., 2005. ATHENA, ARTEMIS, HEPHAESTUS: data analysis for X-ray absorption spectroscopy using IFEFFIT. J. Synchrotron. Rad. 12, 537–541.
Rinklebe, J., Shaheen, S.M., 2017. Redox chemistry of nickel in soils and sediments: a review. Chemosphere 179, 265–278.
Rinklebe, J., Shaheen, S.M., Frohne, T., 2016a. Amendment of biochar reduces the release of toxic elements under dynamic redox conditions in a contaminated floodplain soil. Chemosphere 142, 41–47.
Rinklebe, J., Shaheen, S.M., Schroter, F., Rennert, T., 2016b. Exploiting biogeochemical and spectroscopic techniques to assess the geochemical distribution and release dynamics of chromium and lead in a contaminated floodplain soil. Chemosphere 150, 390–397.
Rizwan, M., Ali, S., Qayyum, M.F., Ibrahim, M., Zia-Ur-Rehman, M., Abbas, T., Ok, Y.S., 2016. Mechanisms of biochar-mediated alleviation of toxicity of trace elements in plants: a critical review. Environ. Sci. Pollut. Res. Int. 23, 2230–2248.
Schulz-Zunkel, C., Rinklebe, J., Bork, H.-R., 2015. Trace element release patterns from three floodplain soils under simulated oxidized–reduced cycles. Ecol. Eng. 83, 485–495.
Shaheen, S.M., Frohne, T., White, J.R., DeLaune, R.D., Rinklebe, J., 2017. Redox-induced mobilization of copper, selenium, and zinc in deltaic soils originating from Mississippi (USA) and Nile (Egypt) River Deltas: a better understanding of biogeochemical processes for safe environmental management. J. Environ. Manage. 186, 131–140.
Shaheen, S.M., Rinklebe, J., Frohne, T., White, J.R., DeLaune, R.D., 2014. Biogeochemical factors governing cobalt, nickel, selenium, and vanadium dynamics in periodically flooded egyptian north nile delta rice soils. Soil Sci. Soc. Am. J. 78, 1065–1078.
Shaheen, S.M., Rinklebe, J., Frohne, T., White, J.R., DeLaune, R.D., 2016. Redox effects on release kinetics of arsenic, cadmium, cobalt, and vanadium in Wax Lake Deltaic freshwater marsh soils. Chemosphere 150, 740–748.
Shen, Z., Hou, D., Jin, F., Shi, J., Fan, X., Tsang, D.C.W., Alessi, D.S., 2019a. Effect of production temperature on lead removal mechanisms by rice straw biochars. Sci. Total Environ. 655, 751–758.
Shen, Z., Zhang, J., Hou, D., Tsang, D.C.W., Ok, Y.S., Alessi, D.S., 2019b. Synthesis of MgO-coated corncob biochar and its application in lead stabilization in a soil washing residue. Environ. Int. 122, 357–362.
Sun, Y., Yu, I.K.M., Tsang, D.C.W., Cao, X., Lin, D., Wang, L., Graham, N.J.D., Alessi, D.S., Komarek, M., Ok, Y.S., Feng, Y., Li, X.D., 2019. Multifunctional iron-biochar composites for the removal of potentially toxic elements, inherent cations, and hetero-chloride from hydraulic fracturing wastewater. Environ. Int. 124, 521–532.
Takeno, N. Atlas of Eh-pH diagrams, Intercomparison of thermodynamic databases, Geological Survey of Japan Open File Report No. 419, 2005. 2005.
Uchimiya, M., Chang, S., Klasson, K.T., 2011. Screening biochars for heavy metal retention in soil: role of oxygen functional groups. J. Hazard. Mater. 190, 432–441.
USEPA, 1994. Method 3051a: Microwave assisted acid digestion of sediments, sludges, soils, and oils.
Wang, Y., Tang, C., Wu, J., Liu, X., Xu, J., 2012. Impact of organic matter addition on pH change of paddy soils. J. Soil Sediment 13, 12–23.

Weishaar, J.L., Aiken, G.R., Bergamaschi, B.A., Fram, M.S., Fujii, R., Mopper, K., 2003. Evaluation of specific ultraviolet absorbance as an indicator of the chemical composition and reactivity of dissolved organic carbon. Environ. Sci. Technol. 37, 4702–4708.

Xing, Y., Wang, J., Shaheen, S.M., Feng, X., Chen, Z., Zhang, H., Rinklebe, J., 2020. Mitigation of mercury accumulation in rice using rice hull-derived biochar as soil amendment: a field investigation. J. Hazard. Mater. https://doi.org/10.1016/j.jhazmat.2019.121747. In press.

Xiong, X., Yu, I.K.M., Cao, L., Tsang, D.C.W., Zhang, S., Ok, Y.S., 2017. A review of biochar-based catalysts for chemical synthesis, biofuel production, and pollution control. Bioresour. Technol. 246, 254–270.

Xu, X., Zhao, Y., Sima, J., Zhao, L., Masek, O., Cao, X., 2017. Indispensable role of biochar-inherent mineral constituents in its environmental applications: a review. Bioresour. Technol. 241, 887–899.

Yang, X., Igalavithana, A.D., Oh, S.E., Nam, H., Zhang, M., Wang, C.H., Kwon, E.E., Tsang, D.C.W., Ok, Y.S., 2018. Characterization of bioenergy biochar and its utilization for metal/metalloid immobilization in contaminated soil. Sci. Total Environ. 640–641, 704–713.

Yoo, J.C., Beiyuan, J., Wang, L., Tsang, D.C.W., Baek, K., Bolan, N.S., Ok, Y.S., Li, X.D., 2018. A combination of ferric nitrate/EDDS-enhanced washing and sludge-derived biochar stabilization of metal-contaminated soils. Sci. Total Environ. 616–617, 572–582.

Yu, I.K.M., Xiong, X., Tsang, D.C.W., Wang, L., Hunt, A.J., Song, H., Shang, J., Ok, Y.S., Poon, C.S., 2019. Aluminium-biochar composites as sustainable heterogeneous catalysts for glucose isomerisation in a biorefinery. Green Chem. 21, 1267–1281.

Yu, K., Böhme, F., Rinklebe, J., Neue, H.-U., DeLaune, R.D., 2007. Major biogeochemical processes in soils-A microcosm incubation from reducing to oxidizing conditions. Soil Sci. Soc. Am. J. 71, 1406–1417.

Yu, K., Rinklebe, J., 2011. Advancement in soil microcosm apparatus for biogeochemical research. Ecol. Eng. 37, 2071–2075.

Yuan, Y., Bolan, N., Prevoteau, A., Vithanage, M., Biswas, J.K., Ok, Y.S., Wang, H., 2017. Applications of biochar in redox-mediated reactions. Bioresour. Technol. 246, 271–281.